# Preventing Oxidation of Aluminum Mirrors with Cadmium and Zinc Barriers

Stephanie Thomas

A senior thesis submitted to the faculty of
Brigham Young University
in partial fulfillment of the requirements for the degree of

Bachelor of Science

David D. Allred and R. Steven Turley, Advisors

Department of Physics and Astronomy

Brigham Young University

April 2017

ABSTRACT

Preventing Oxidation of Aluminum Mirrors with Cadmium and Zinc Barriers

Stephanie Thomas
Department of Physics and Astronomy, BYU
Bachelor of Science

Pure aluminum mirrors optimize the reflectance of broadband mirrors for space-based telescopes; however, they oxidize instantly in atmospheric conditions, decreasing reflectance in the far-UV from 90% to 20%. The largely untried method of Removable Volatile Aluminum Protection (REVAP) overcoats freshly deposited Al mirrors with a barrier layer of cadmium or zinc intended for removal in vacuum. I use ellipsometry and energy dispersive x-ray spectroscopy (EDS) periodically to observe how the barrier layers interact with the Al and how the composition of the mirrors changes with time. Preliminary EDS results show Cd may have prevented aluminum oxidation in some samples. Cd and Zn exhibit low adhesion to Al, making REVAP with them unfavorable. EDS measurements on samples after attempting re-evaporation shows uneven removal of Cd and Zn.

Keywords: aluminum, cadmium, zinc, oxidation, REVAP, space-based telescopes

# ACKNOWLEDGMENTS

There's nothing “easy" about physics research. In my time as an undergraduate researcher, I have encountered significantly many more failures than successes. I've learned that the key is recognizing that each ‘failure’ is a learning experience and a stepping stone to continuously move forward. In moments of discouragement, there are no better motivators than Dr. Allred and Dr. Turley. They are two of the most patient, optimistic, and enthusiastic advisors and I am grateful for their dedication and support of me as I stumbled through this major.

I would never have been given this opportunity had it not been for my teacher, mentor, and friend David Balogh. His genuine enthusiasm for science inspired me to pursue a degree in Physics and his recommendation led me here. I would never have been able to come here–to learn, to explore, to grow–if it were not for Mr. Balogh. I am considerably humbled by his support and feel it would be a dishonor to neglect such an influential figure in my educational career.

# Contents

# Chapter 1

# Introduction

Far-ultraviolet light is of significant interest in space applications for many reasons. For this narrow range of light, resting between approximately $120-200$ nanometers in wavelength ($6.2-12.4$ electron-volts) on the electromagnetic spectrum, most materials possess a relatively large imaginary component in their indices of refraction. This imaginary component indicates that materials, including atmosphere, will absorb the light, making it difficult to study on Earth. The light is abundant in space, however, as it is emitted by high-energy sources. For example, 30.4 nm light is radiated from the solar corona and reflects from singly ionized helium trapped by the plasmasphere.

In 2000, NASA launched the Imager for Magnetopause-to-Aurora Global Exploration (IMAGE), a satellite with the purpose of imaging the plasmasphere [1]. It made use of an alternating uranium-silicon thin film multilayer to detect the light from the solar corona after being reflected from the singly-ionized helium in the plasmasphere. This allowed researchers to "see" the plasmasphere; Figure 1.1 shows a generated image of it from the satellite.

More ambitious is the Large Ultraviolet-Optical Infrared space-based observatory (LUVOIR), which could be equipped with a primary telescope mirror up to 16 meters in diameter [3]. The BYU Extreme Ultraviolet (XUV) Group is determined to provide a thin-film multilayer mirror design for this telescope that will extend its broadband reflectance capabilities into the far-UV

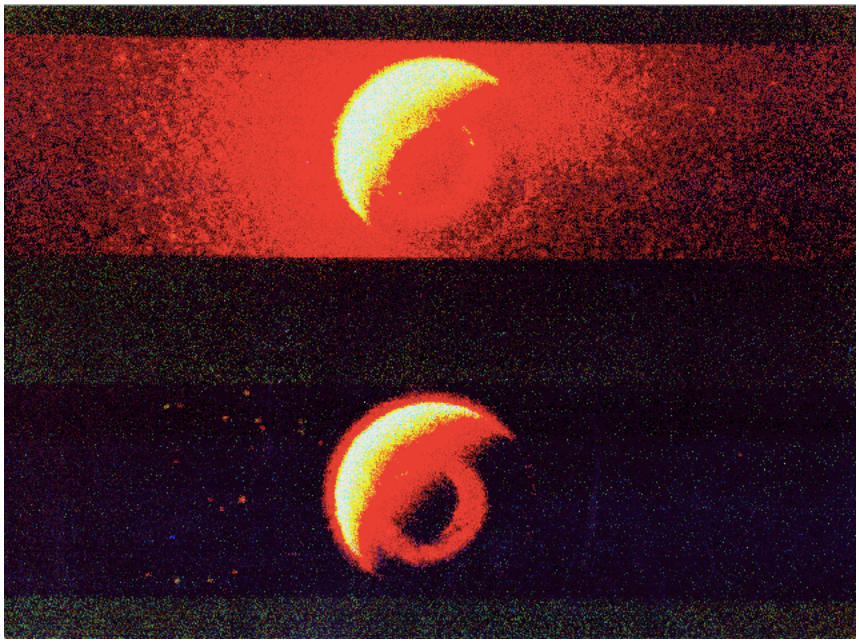

**Figure 1.1** Simulated view of the Earth's aurora as seen by IMAGE. *Source: NASA [2]*

and XUV. The group is exploring various methods to achieve this. My project focused on using aluminum as the outermost reflective layer of a (yet undetermined) multilayer composition.

To keep the Al layer from oxidizing, I investigate Removable Volatile Aluminum Protection (REVAP) [4]. This method suggests using volatile metals (i.e. metals with significantly lower vapor pressures than Al) as a barrier layer between Al and atmosphere. This barrier layer would then be removed by direct application of heat in outer space. Should REVAP prove to be effective and applicable, it would push the range of detectable light further into the far-UV than the current standard, aluminum/magnesium fluoride ($Al/MgF_2$) or aluminum/aluminum fluoride ($Al/AlF_3$) multilayer mirrors.

Here I will discuss the background information, processes, and results of my efforts. In this chapter, I explain why Al is more desirable than $Al_2O_3$ for broadband reflectance, how the method of REVAP is applied, and associated references and research projects. The second chapter I have dedicated to the experimental method; I will describe evaporation deposition, characterization tech-

niques, and re-evaporation. In the final chapter, I present the results and their implications, then conclude with suggestions for further research.

By the end of this thesis, I will address the following two questions: Is a cadmium or zinc removable barrier layer effective in protecting Al mirrors? Is the barrier layer completely removed by re-evaporation?

I will now describe the motivation for my project.

## 1.1 Motivation

Broadband reflectance of space-based telescopes and observatories is attainable with Al mirrors; however, the reflectance of the mirrors decreases significantly with the introduction of oxygen. This feature makes it difficult to manufacture such mirrors for telescopes, as when left unprotected they quickly interact with oxygen in atmosphere. This provides researchers with opportunities to fabricate alternative methods.

In 1983, W. M. Burton proposed a largely unexplored method of removable mirror protection, Removable Volatile Aluminum Protection (REVAP), and recommended cadmium and zinc as candidates for the method based on their fulfillment of specific parameters [4]. I experimentally determine the practicality and reliability of this method by making protected Al mirrors using evaporation deposition in a Denton thermal evaporator and measuring them with ellipsometry, scanning electron microscopy (SEM), and energy dispersive xray spectroscopy (EDS).

The motivation to test this method is to design a broadband mirror for space-based telescopes, such as the Large Ultraviolet-Optical-Infrared (LUVOIR) Surveyor, which would use a broadband telescope for enhanced space exploration. Al mirrors reflect far-UV light, which would allow the LUVOIR to detect earth-like planets in other solar systems.

The convenience of a bare Al mirror is met with a significant inconvenience: Bare Al oxidizes

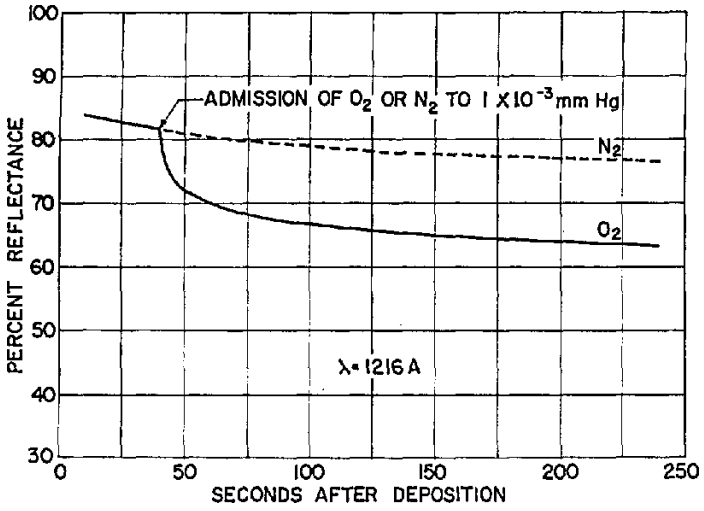


**Figure 1.2** The reflectance of Al immediately after deposition and with the introduction of $1 * 10^{-3}$ mm Hg (equivalent to $1.0 * 10^{-6}$ atm) oxygen ($O_2$) gas. There is an abrupt change in rate of reflectance vs. time at approximately 35 s, when $O_2$ is introduced into the chamber. [5]

instantly, decreasing the mirror's reflectance in the far-UV. The next section will discuss this in more detail.

## 1.2 Aluminum vs. Aluminum Oxide

Al is desirable for telescope mirrors; however, it oxidizes immediately in oxygen-containing atmosphere (see figure 1.2). Figure 1.2 shows the reflectance of Al at 121.6 nm immediately after deposition. The introduction of nitrogen gas ($N_2$) does not appear to change the trend of decreasing reflectance, but when $O_2$ is introduced, the reflectance sharply drops before returning to its previous trend at a lower amplitude. The $O_2$ immediately interacts with the Al surface, dramatically affecting reflectance in the far-UV.

Figure 1.3 shows why it is important to counter atmospheric interaction. The reflectance in the far-UV of Al is ranges from $80 - 90\%$ while the reflectance of Al overcoated with only 5 nm $Al_2O_3$ is less than 20%. The figure indicates two points of interest: 85 nm and 72 nm. At 85

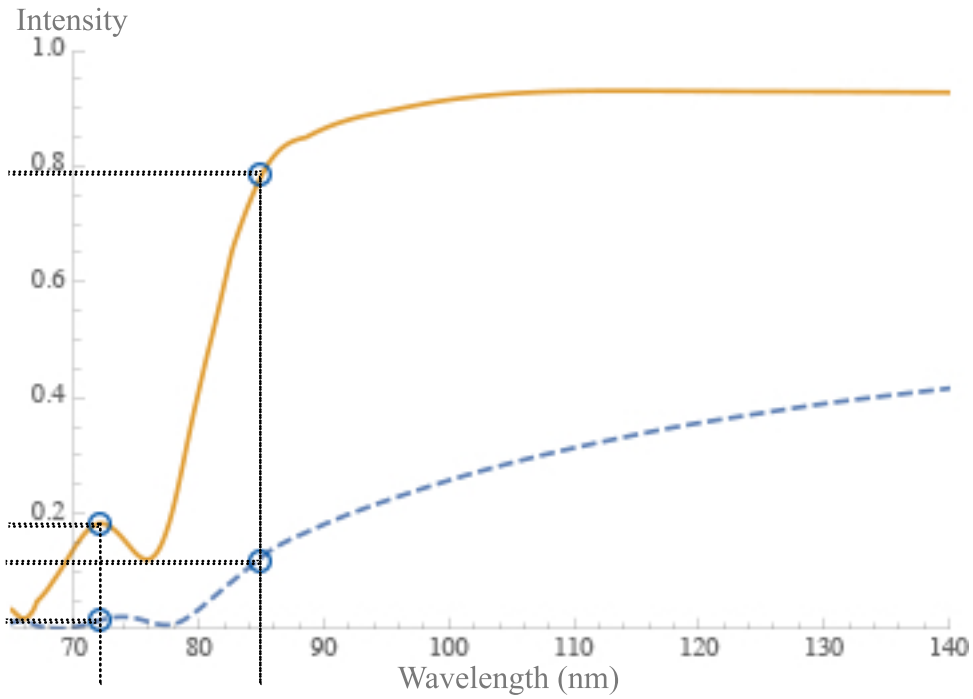


**Figure 1.3** Comparison of reflectance vs. wavelength for 100 nm Al and 100 nm Al/5 nm $Al_2O_3$ on Si at incident angle $\theta = 80°$ from grazing. The reflectance of Al is approximately 80% at 85 nm with an additional peak of 20% reflectance at 72 nm. Compare to the Al/$Al_2O_3$ mirror, which is less than 20% reflective at the same wavelengths.

nm, the reflectance of Al begins to approach its maximum. The smaller wavelengths show strong reflectance compared to $Al_2O_3$, especially between $70-90$ nm. Another benefit of bare Al is the small peak in the XUV, at about 72 nm.

A bare Al front-surface mirror will extend the range of accessible light to 85 nm, with an additional small peak in the extreme ultraviolet due to the multilayer interface. At wavelengths smaller than 85 nm, the series of mirrors of the observational instrument causes too much of the light to be absorbed or dissipated before it reaches the detector, and is therefore inefficient.

To access the wavelengths allowed by bare Al front-surface mirrors, it is necessary to prevent oxidation. Even a thin layer of surface oxidation causes significant reflectance loss, as figure 1.3 indicates. Several options are available for researchers to explore, but they ultimately reduce to these: either make the mirror on Earth or make it in space. I explore a method that draws elements

**Table 1.1** The calculated vapor pressures of Al, Cd, and Zn at high and low temperatures. *Source: Institut für Angewandte Physik, Technischen Universität Wien* [6]

| Element | Torr at 20°C | Torr at 200°C |
|---|---|---|
| Aluminum | $1.69 \times 10^{-49}$ | $3.69 \times 10^{-27}$ |
| Cadmium | $1.09 \times 10^{-11}$ | $3.66 \times 10^{-4}$ |
| Zinc | $7.38 \times 10^{-15}$ | $4.59 \times 10^{-6}$ |

from both options, which I will now discuss in detail.

## 1.3 REVAP

Removable Volatile Aluminum Protection (REVAP) is the method of protecting Al mirrors from oxidation in atmosphere by depositing volatile barrier layers intended for removal by evaporation in space [4]. In an ultrahigh vacuum evaporator, Al coats a Si substrate immediately before a thin, protective layer overcoats it. This protective layer must meet certain qualifications, outlined below. The layer is then removed under vacuum, such as the vacuum of outer space. The method of removal I consider is thermal re-evaporation, but the XUV Group also contemplates chemical removal.

Potential barrier layers must:

- not interact with or degrade Al,
- have low vapor pressure at low temperatures, and
- have high vapor pressure at high temperatures.

Two candidates that fit these parameters are cadmium and zinc. Cd forms no compounds or alloys with Al and Burton concluded that Zn did not interfere with the Al in the visible or near

UV [4]. Table 1.1 shows the relative calculated vapor pressures at 20°C and 200°C of Al, Cd, and Zn. The vapor pressure of Cd and Zn differ from Al by several orders of magnitude. At either temperature indicated on the table, an impossible pressure would need to be achieved to risk vaporizing Al in the re-evaporation process. Pressures in the order of magnitude for Cd and Zn at high temperatures are easily attainable in the Denton.

Due to the toxic properties of Cd, Burton opted to use Zn as a barrier layer. He used evaporation deposition to produce the mirrors which consisted of two partially overlapping regions of Al and Zn. After measuring the thickness of the Al-Al/Zn-Zn REVAP sample with a microdensitometer, he re-evaporated the Zn *from* the sample, then measured the remaining thickness. "The residual optical density in the region originally coated only with zinc but subsequently 'revaporated' can be seen to have returned essentially to its initial uncoated value, indicating that the zinc coating has been completely removed from the surface. [4]"

This method was designed to allow astronomers to access the far-UV with bare Al mirrors. While it has been largely untested, many researchers have considered alternative methods of unlocking the far-UV with Al. I describe a handful of related projects in the next section.

## 1.4 Past/Concurrent Research

The IMAGE Mission (Mar. 2000-Dec. 2005), as mentioned previously, used a multilayer thin film mirror of alternating silicon and uranium to visualize and characterize the plasmasphere [1]. Expounding on this concept, accessing the far-UV with large Al telescopes would allow for the detection of a plasmasphere surrounding earthlike exoplanets. This is significant because the presence of a plasmasphere may indicate a stable atmosphere as well.

NASA will soon discuss four candidates for their next flagship space-based observatory. One of the candidates is a Large UV-Optical-IR (LUVOIR) Surveyor from the Goddard Space Flight

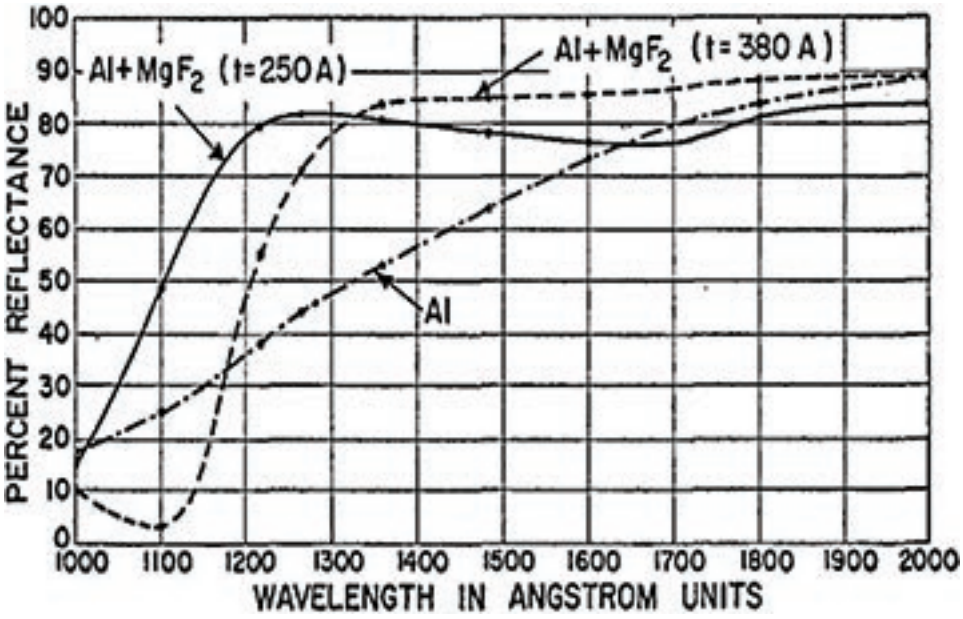


**Figure 1.4** Comparison of reflectance in the far-UV of bare Al, Al/25 nm $MgF_2$ , and Al/38 nm $MgF_2$. [8].

Center [7]. The LUVOIR could have a broadband mirror up to 16 m in diameter [3]. Such a large telescope, if equipped with a bare Al outermost reflecting layer, would be ideal for plasmasphere detection as mentioned.

The current standard to overcome the decreased reflectance caused by oxidation is to use mirrors of Al overcoated with $MgF_2$ or $AlF_3$. These fluorides extend the range of wavelengths for high reflectance beyond the range of mirrors coated with $Al_2O_3$, but not as far as bare Al. For reference, the reflectance of Al/$MgF_2$ compared to bare Al is shown in Figure 1.4. The plot shows high reflectance of the Al/$MgF_2$ samples at wavelengths greater than approximately 120 nm, but absorption effects cause a large decrease in reflectance at smaller wavelengths.

The BYU XUV Group is working together with this purpose: to get broadband, bare Al mirrors into orbit. Margaret Miles, a graduate student, is designing an evaporation deposition system within a monochromator to take reflectance measurements of freshly evaporated Al. Michael Greenburg is optimizing a genetic algorithm to determine the most effective multilayer compo-

sition for the mirrors. Spencer Thevenin is computationally characterizing the effect of surface roughness for far-UV reflective mirrors. Spencer Willett is testing a method of chemical removal of polymer barrier layers (as an alternative to Cd and Zn) using hydrogen plasma.

I use REVAP to deposit - and later remove - metal barrier layers of Cd or Zn on Al mirrors to test if the Al is unchanged over time and if the barrier layers can be removed. I will now describe the process I used to show these.

# Chapter 2

# Experimental Method

The three main steps for this project are to deposit the mirrors and barrier layers, characterize them over time, and then remove the barrier layers. In making the mirrors, selecting and preparing the substrates was the first task. The Al and Cd/Zn were deposited sequentially *in situ* in the Denton evaporation deposition system. Promptly, I made an initial optical characterization of the samples with ellipsometry, then made several subsequent measurements throughout the following week to compare changes in reflectance over time. Scanning electron microscopy (SEM) and energy dispersive xray spectroscopy (EDS) characterize the mirrors structurally and chemically. After the measurements had been completed, I returned the samples to the Denton for re-evaporation. I used SEM and EDS again to characterize the 'revaporated' samples. Because the barrier layer had been removed, the Al was compromised and ellipsometry was unnecessary. SEM and EDS provided information about how completely the Cd or Zn had been removed from the Al. Each of the steps is now described in detail.

## 2.1 Substrates

To make the mirrors, I first needed to select and prepare substrates. The substrates I chose were either silicon (Si) based or quartz. The Si wafers were prepared previously with thin coatings of $SiO_2$ or $Si_3N_4$. These layers acted as interference layers to assist in spectroscopic characterization. The quartz slides, dielectrics, were bare and selected for spectroscopic characterization as well; however, the quartz was chosen for its transparency to allow direct optical access to aid in ellipsometric characterization. They were to be viewed from the underside, through the dielectric, in a process called back-surface ellipsometry (2.4).

I divided the substrates into groups for deposition. There were five groups total, each classified by the composition of their specific barrier layers. The first three groups, intended for Cd/Al samples, each had a quartz microscope slide and a 1-mm-thick Si wafer with an interference layer (Si+IL) substrate. It was initially believed that the three Si substrates had the same interference layer, 150 nm $Si_3N_4$; however, it was later discovered that Group II and Group III had $Si_3N_4$ while Group I had 150 nm $SiO_2$. Groups IV and V were Al/Zn samples. For these, three substrates were set apart: a quartz slide and two Si+IL wafers. The Si+IL layers were both $SiO_2$, of different thickness. I drew one of the substrates for Groups IV and V from the same source as the substrate from Group I, so having two $SiO_2$ samples was not intended. These $SiO_2$ interference layers (found in Groups I, IV, and V) were 150 nm thick, and the others (which I refer to as "thick" $SiO_2$) were 1$\mu$m. For a collected reference of the grouping of each sample, refer to Table 2.1.

Once I had gathered the substrates, I began the deposition process.

## 2.2 Evaporation Deposition

I made twelve samples, in groups of two or three substrates at a time (see Table 2.1). The sample compositions can be found in Tables 2.2 and 2.3. I used a Denton (model DV-502 A) thermal

**Table 2.1** Quick-reference of the division of substrates in five groups for deposition. An * indicates "thick" $SiO_2$ ($1\mu$m thickness).

| Group | I | II | III | IV | V |
|---|---|---|---|---|---|
| Barrier | Cd | Cd | Cd | Zn | Zn |
| Substrate | Quartz<br>Si+$SiO_2$ | Quartz<br>Si+$Si_3N_4$ | Quartz<br>Si+$Si_3N_4$ | Quartz<br>Si+$SiO_2$<br>Si+$SiO_2$* | Quartz<br>Si+$SiO_2$<br>Si+$SiO_2$* |

evaporation deposition system to fabricate them.

The Denton was a necessary choice for testing REVAP for many reasons. First, it contains two independently controlled pairs of electrodes for evaporating the sources. Utilizing both of these, I evaporated Al onto the substrates and then followed with barrier layer quickly afterward without breaking vacuum. Quick action was an important factor as well; Figure 1.2 shows that oxidation occurs even in high-vacuum. This is merely a limitation of technology (as we cannot achieve perfect vacuum), but its impact is lessened by acting quickly. By performing the depositions without breaking vacuum between depositions, oxidation was further prevented. A third reason the Denton was a necessary choice is that it is a system that operates under high-vacuum ($1-10\mu$Torr). Operating under high vacuum minimizes interactions between the source and other particles in the chamber, which ensures a smooth, uniform, deposited surface.

Figure 2.1 identifies the key components of the Denton evaporator. Point A is the stage, where the substrates are placed face-down. B points to the shutter, which controls the access of the evaporated material to the substrates. It is controlled by C, the quartz-crystal monitor. This measures the thickness of the deposited layer in realtime and can be programmed to operate the shutter as desired. Two pairs of electrodes, indicated by D, are positioned on either side at the base of the

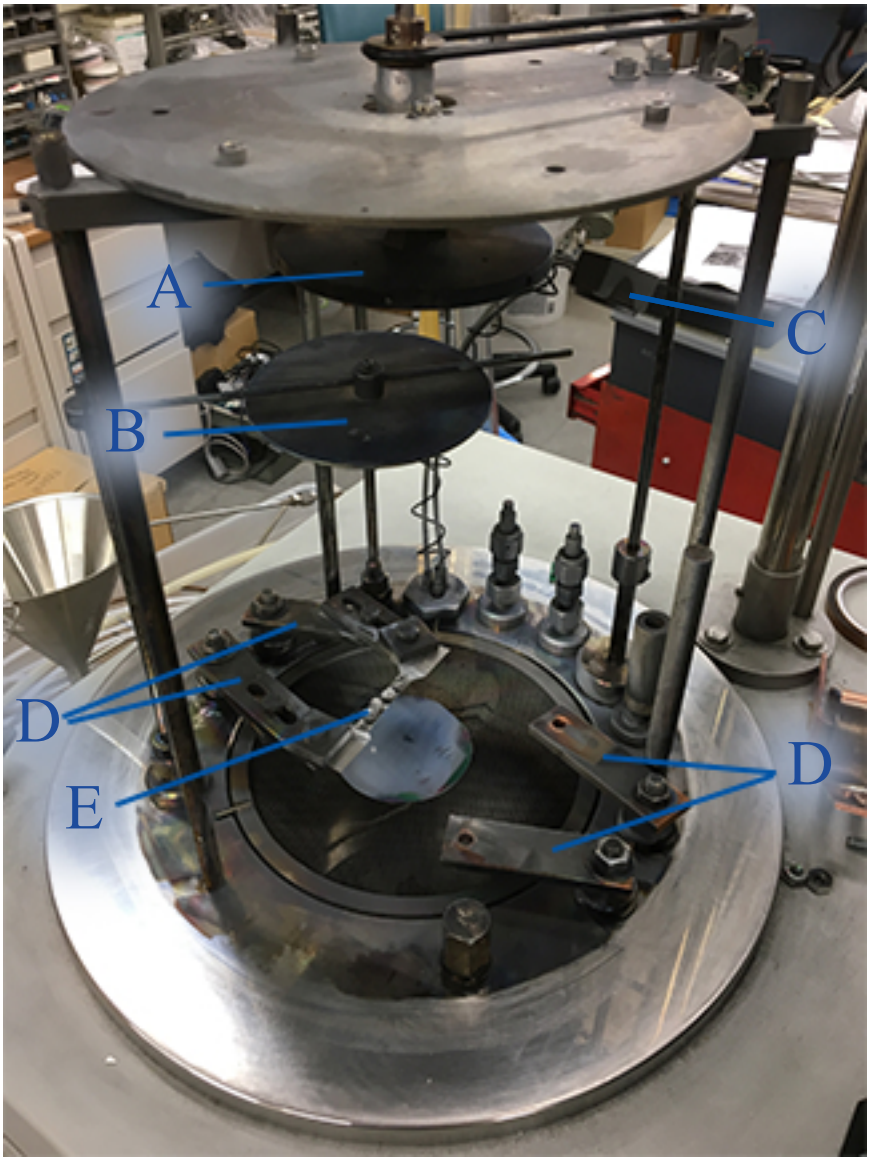


**Figure 2.1** The inner chamber of the Denton evaporator. The points of interest are indicated: A points to the stage, B points to the shutter, C points to the quartz-crystal monitor, D points to the two pairs of electrodes, and E points to the source material.

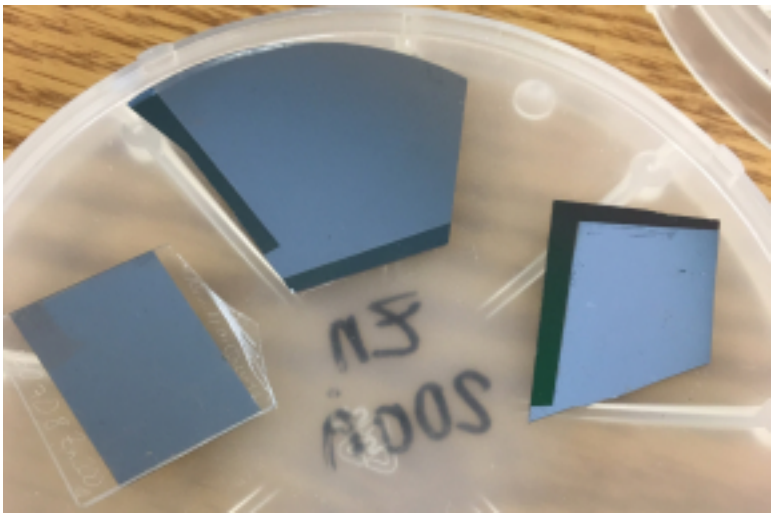

**Figure 2.2** Samples 10, 11, and 12 post-deposition. From the left: Sample 12 (quartz with 20 nm Zn), Sample 11 (150 nm $SiO_2$ with 20 nm Zn), and Sample 10 (1 000 nm $SiO_2$ with 20 nm Zn).

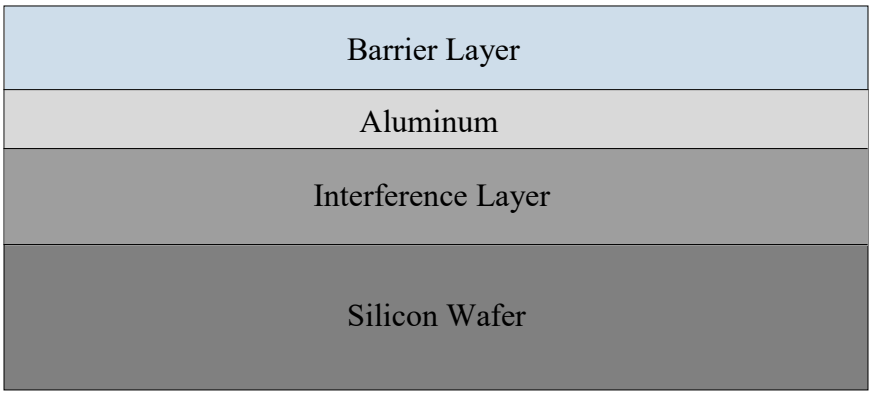


**Figure 2.3** Diagram of the cross-sectional area of the samples grown on Si wafers.

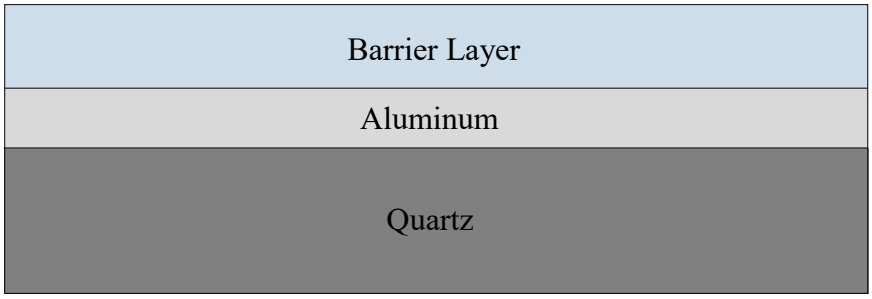


**Figure 2.4** Diagram of the cross-sectional area of the samples grown on quartz slides.

chamber, and can be controlled independently. Between the first pair of electrodes, as point E shows, is a source held by a tungsten boat. A tungsten coil may also be placed between the electrodes and was preferred for the thin Al wire I used as a source. For Cd and Zn, which were in the form of small pellets, a tungsten boat was sufficient. (More detailed instructions about sample fabrication with the Denton can be found in Appendix A.)

For each group of substrates, the deposition process was straightforward. After the chamber reached a pressure between $6-9\mu$Torr, I began to run a current corresponding to $20-35\%$ power through the first pair of electrodes, containing the Al source. The shutter was closed to begin, but when the metal began to evaporate, I opened it, exposing the substrates to the vaporized Al. When the desired nominal thickness of Al (3 nm for Groups I, II, and III and 10 nm for Groups IV and V) had coated the sample, the shutter closed automatically (see appendix A) and I switched the flow of current from the first pair of electrodes to the second, which were connected to the barrier layer source. Following the same pattern, I opened the shutter when the metal began to evaporate and it closed automatically when the desired nominal thickness had coated the Al. Upon completing the deposition, I shut off the current and vented the chamber with $N_2$ gas. This process was repeated for all five groups of substrates.

Figures 2.3 and 2.4 show the cross-sectional area of the layers of the Si samples and quartz sam-

**Table 2.2** Nominal sample composition of samples in Groups I, II, and III (the Al/Cd groups). Layer thicknesses are measured in nanometers (nm).

| Sample | 1 | 2 | 3 | 4 | 5 | 6 |
|---|---|---|---|---|---|---|
| Substrate | Si+$SiO_2$ | Quartz | Si+$SiO_2$ | Quartz | Si+$SiO_2$ | Quartz |
| Al (nm) | 3 | 3 | 3 | 3 | 3 | 3 |
| Cd (nm) | 5 | 5 | 7.5 | 7.5 | 10 | 10 |

**Table 2.3** Nominal sample composition of samples in Groups IV and V (the Al/Zn groups). Once again, the * indicates $SiO_2$ thickness of 1$\mu$m. Layer thicknesses are measured in nanometers (nm).

| Sample | 7 | 8 | 9 | 10 | 11 | 12 |
|---|---|---|---|---|---|---|
| Substrate | Si+$SiO_2$* | Si+$SiO_2$ | Quartz | Si+$SiO_2$* | Si+$SiO_2$ | Quartz |
| Al (nm) | 10 | 10 | 10 | 10 | 10 | 10 |
| Zn (nm) | 10 | 10 | 10 | 20 | 20 | 20 |

ples, respectively. Figure 2.2 is a picture of Group V, post-deposition and prior to re-evaporation.

I will now discuss the re-evaporation process.

## 2.3 Re-evaporation

The first step of REVAP was to coat the Al mirrors with Cd or Zn; the next step was to show that the barrier layer could be removed completely [4]. Ideally, the barrier layer would leave the Al mirrors smooth and unchanged. In other words, it would leave the Al as-deposited–free of oxidation and highly reflective in the far-UV.

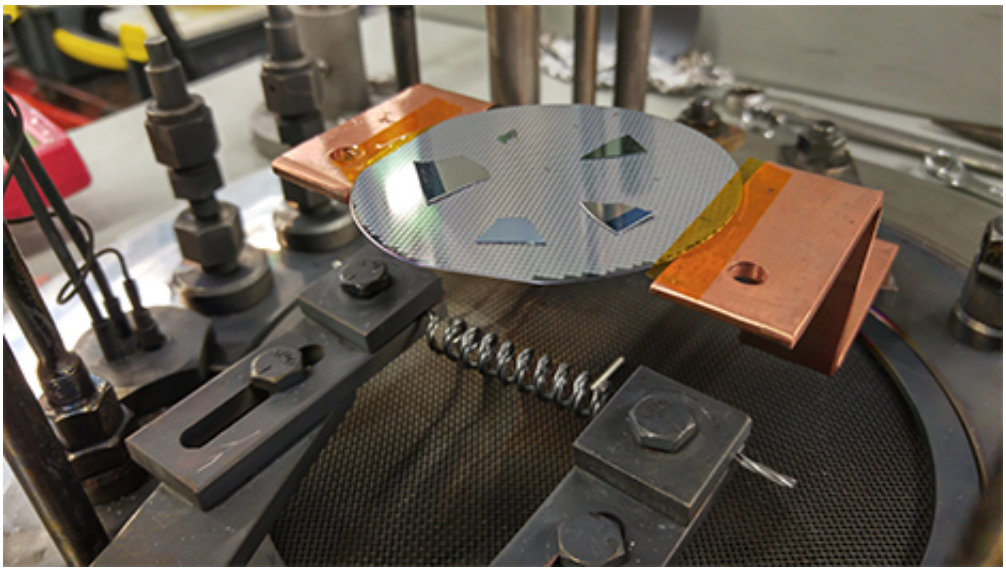

**Figure 2.5** Modification to the Denton for re-evaporation. Copper bars hold a Si wafer topped with pieces of samples over a tungsten coil secured between the other pair of electrodes.

I began by testing thermal re-evaporation within the Denton evaporator. Figure 2.5 shows the re-evaporation setup. Copper extensions were machined and attached to one of the pairs electrodes (figure 2.1), creating an elevated platform. A Si wafer was secured between the copper pieces and small pieces of the samples were placed on top. Underneath the elevated samples was a tungsten coil attached to the other pair of electrodes. A current was manually turned on through the coil and resistance in the coil generated heat, which evaporated the barrier layers from the samples placed above it without affecting the Al. Al was unaffected because of the relative vapor pressures of Cd, Zn, and Al, as shown in Table 1.1. The samples were left in the heated Denton for either 15 or 30 minutes. Table 2.4 outlines the parameters used for re-evaporation of the samples. Not every sample was re-evaporated.

Once the samples were re-evaporated, they were ready for post-REVAP characterization. The methods of characterization I used for post-REVAP samples were scanning electron microscopy (SEM) and energy-dispersive xray spectroscopy (EDS), explained in detail in the next section.

**Table 2.4** REVAP current percentages and times for selected samples.

| Sample | Current (%) | Time (min.) |
|---|---|---|
| 1 | 30 | 30 |
| 3 | 70 | 15 (twice) |
| 5 | 30 | 30 |
| 7 | 30 | 30 |
| 10 | 70 | 15 |

## 2.4 Characterization

The samples were characterized using processes that I will not explain in too much detail here, but have explained in Appendix B.

### 2.4.1 Ellipsometry

I measured each Si-based sample (Samples 1, 3, 5, 7, 8, 10, and 11) on a J. A. Woollam ellipsometer (see Appendix B) multiple times: first, directly after deposition and then again several times over the next few days. I took the data from five different angles: 60°, 65°, 70°, 75°, and 80°, in order to include the quasi-Brewster's angle (which can be calculated, but was only estimated for this project as being somewhere between $60-80°$) in the scans. Figure 2.6 shows the data collected over time for Sample 5 (Cd 10 nm on Si/$Si_3N_4$, see Table 2.2). I did not measure the quartz substrate samples with this method. The layers were so thin that the data was unreliable, possibly due to internal and back-surface reflections. The quartz samples (Samples 2, 4, 6, 9, and 12) were instead reserved for transmission scans and back-surface ellipsometry.

I used back-surface ellipsometry (BSE) (figure 2.7) to measure the quartz samples from the

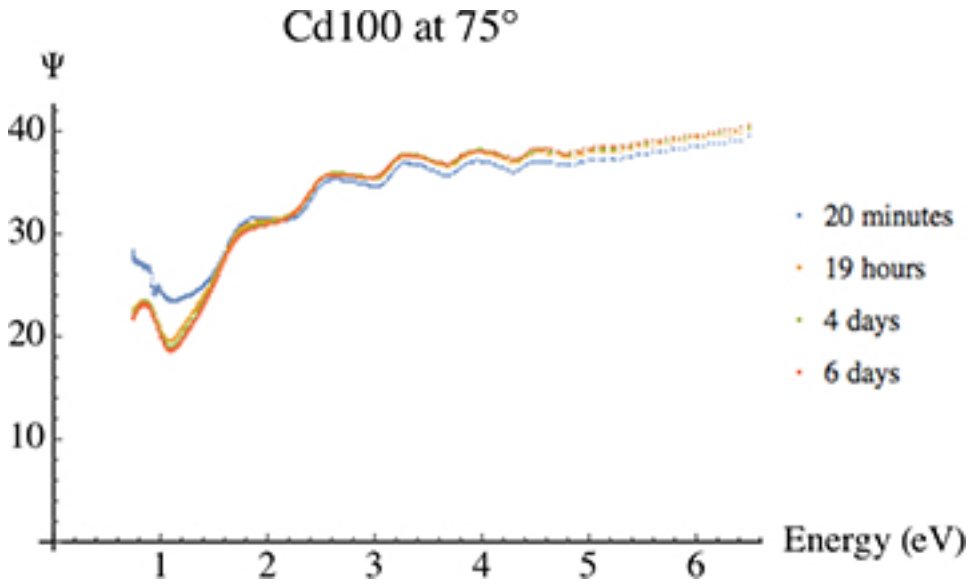


**Figure 2.6** Energy (eV) vs. $\tan\Psi$ (Eq. B.5) of Sample 5 (Cd 10 nm on $Si/Si_3N_4$) taken at 20 minutes, 19 hours, 4 days, and 6 days over a range of $1-7$ eV at incident angle $75°$.

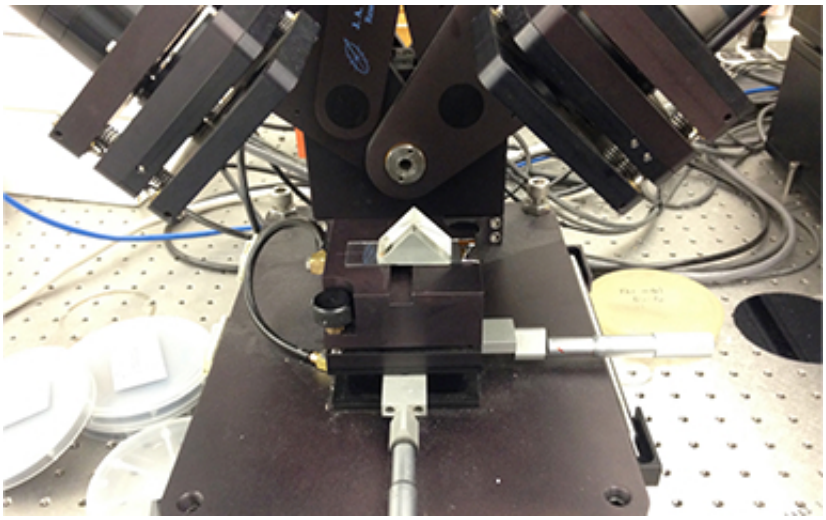

**Figure 2.7** The set-up for back-surface ellipsometry (BSE). The quartz sample is placed upside down on the stage of the ellipsometer (in the center) and a $30-30-120°$ quartz prism is placed on top of it, as shown.

underside. For BSE, the sample was placed upside-down at the center of the stage and a quartz prism ($30-30-120^{\circ}$) was placed on top. The prism acted as an environment-matching material for the quartz slide to limit internal reflections of light from the wide incident angles.

A third variation of optical measurement I used was transmission using the ellipsometer. Each transmission scan gathered data measured in much the same way as in reflective ellipsometry described above, except it used transmission coefficients rather than reflection coefficients. This was performed by sending light at normal incidence through the sample, which was centered by a make-shift stage just before the detector, and measuring the transmitted intensity.

The purpose of measuring the samples with reflective ellipsometry, back-surface ellipsometry, and transmission scans was to observe qualitatively the change in the samples over time. If the reflectance changed, the implication was that something within the sample was changing. Change could imply oxidation–which figure 1.2 shows, decreases the reflectance of Al. If the Al oxidized, the Cd and Zn did not effectively protect it. However, simply visualizing a change was not enough to determine whether the project failed or succeeded; I needed quantitative data as well. I used the scanning electron microscope and energy-dispersive xray spectroscopy to acquire this.

### 2.4.2 Structural Imaging and Chemical Characterization

Scanning electron microscopy (SEM) and energy dispersive xray spectroscopy (EDS) allowed me to acquire both qualitative and quantitative data about the Si-based samples. These were Samples 1, 3, 5, 7, 8, 10, and 11 (Tables 2.2 and 2.3). Quartz samples were not measured with SEM or EDS because strong reflection is required; quartz is transparent to the electron beam and the beam reflected strongly from the sample holder instead.

With the SEM, I structurally characterized of areas approximately $1.5\mu m^2$. Figure 2.8 shows an example of an image generated for Sample 5 by the SEM.

EDS generated a percent atomic composition of a small volume of the samples. Figure 2.9

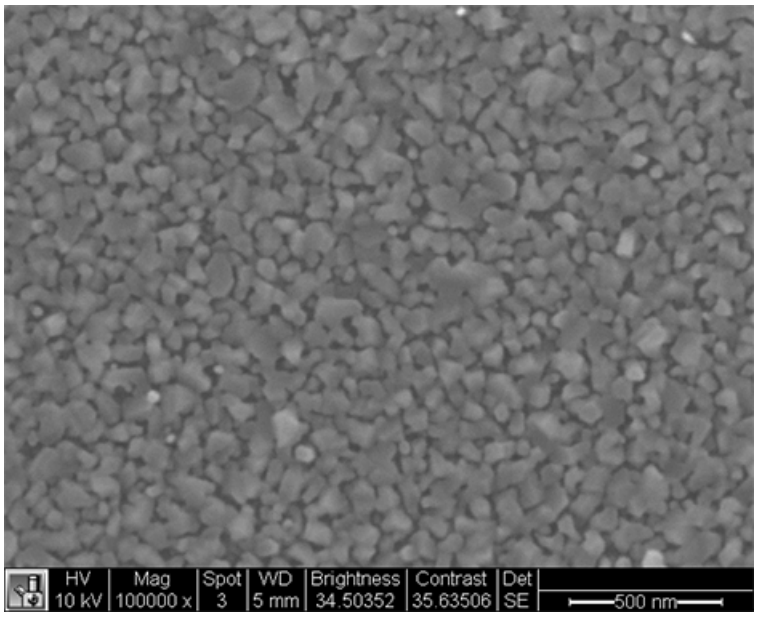


**Figure 2.8** SEM produced image of Sample 5 (Table 2.2) with beam strength 10 kV over $1.5\mu m^2$.

shows the EDS results, a histogram of photon energy counts, for Sample 5. The peaks in the histogram indicate the number of counts of emitted photons at each energy, which are correlated to well-known transition energies for each element to determine the atomic composition (appendix B).

The Si-based samples were measured with SEM and EDS both before and after REVAP. Beforehand, I determined how well the Al was protected by the barrier layer and observe the surface structure of the samples. Afterward, I determined how much of the barrier layer had remained after attempting to re-evaporate it. In the next chapter, I will discuss the results of these measurements.

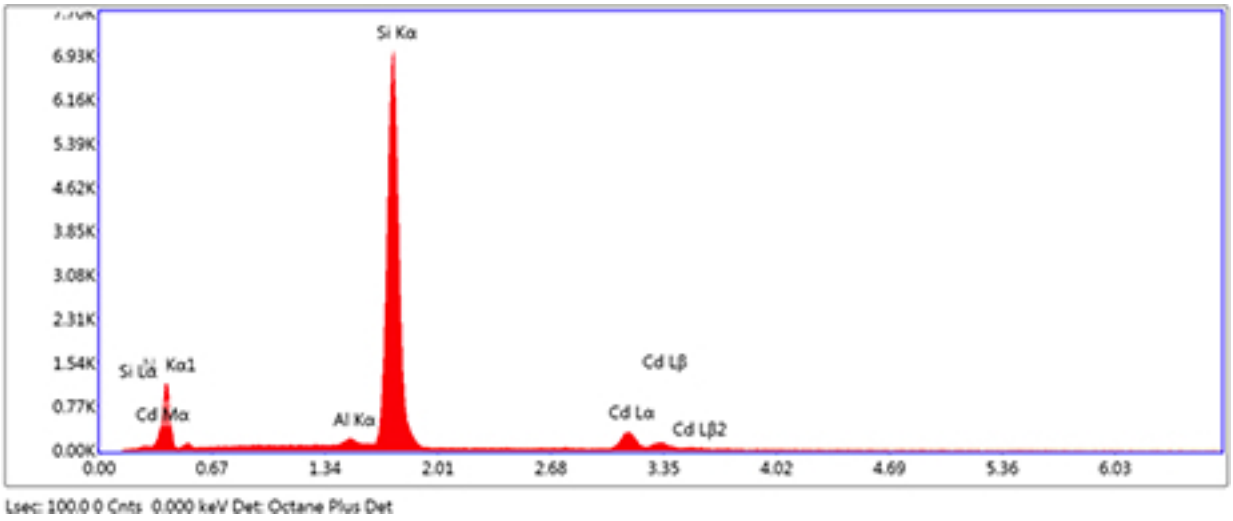


**Figure 2.9** EDS histogram of photon energy counts for Sample 5 (Table 2.2) with beam strength 10 kV $\mu$m$^2$. Notice the peaks around 3.2 eV (Cd L$\alpha$), 1.5 eV (Al K$\alpha$), 0.4 eV (N K$\alpha$), and 1.8 eV (Si K$\alpha$). The composition of this sample was Si, N, Al, and Cd.

# Chapter 3

# Results and Discussion

Several of the samples had unfavorable substrate compositions. Therefore, Samples 3 and 5 (2.2) will be the focus of my analysis and conclusions. The results from these two samples are modest and primarily speculative; however, they lay some groundwork for advancement in this field of research. Sample 3 and Sample 5, consisting of 7.5 and 10 nm Cd barrier layers, respectively, were measured pre-REVAP with ellipsometry, SEM, and EDS and post-REVAP with SEM and EDS. Post-REVAP, they were not measured with ellipsometry as they were exposed to oxygen-containing atmosphere upon Cd removal and oxidized instantly.

Pre-REVAP results of Samples 3 and 5 show that there is some interaction occurring beneath the Cd barrier layer over time, although there is uncertainty as to what these interactions are. Frequent ellipsometric scans show a change over time of the ratio of s- and p-polarized light intensity upon reflection (3.1, 3.2), suggesting the interactions previously mentioned. The SEM measurements produced an image of the sample surfaces that were visibly rough (3.3, 3.4), suggesting possible “pathways" for $O_2$ to reach the Al underneath the Cd. Finally, an EDS scan for each sample predicted an atomic composition excluding $O_2$ (3.1). This suggests that although ellipsometry predicted interactions within the sample, oxidation may not have been one of them.

The re-evaporation method I tested requires refining. As I mentioned previously, Samples 3

and 5 were not measured with ellipsometry post-REVAP due to their certain oxidation; however, visual inspection of Sample 5 suggests the Cd barrier layer was removed unevenly from the surface (3.6). I measured each of the points indicated in Figure 3.6 with EDS, obtaining a relative atomic percent composition confirming that the Cd was indeed removed unevenly (3.7, 3.8, 3.9). Sample 3 was not characterized post-REVAP.

I will now discuss the results of my experiment and conclude with suggestions for further work.

## 3.1 Discussion

### 3.1.1 Characterization Methods

The phase changes of the sample, measured by ellipsometry over time, allowed for a loose conclusion: the composition of the samples changed over time. The ratio of the amplitudes of reflected p- and s-polarized light intensity is represented by $\tan(\Psi) = |R_p|/|R_s|$. A Cauchy model, a generic model used to characterize the reflectance trend, was used to try to fit the data. Unfortunately, the samples were so rough that fitting the data to a model was unreliable and inconsistent. Back-surface ellipsometry, insofar as I was able to use it, also did not provide useful data.

Figures 3.1 and 3.2 show that the samples changed over time. I measured the samples at five incident angles (from $60-80^o$ in increments of $5^o$) at 4.5 eV. The angles were chosen to include the quasi-Brewster angle and for large-angle reflectance measurements. The energy, corresponding to approximately 275 nm, was selected because it is in the UV range. The plots in Figures 3.1 and 3.2 show an initial increase in $\Psi$, then the slope levels out as time increases. The values of $\Psi$ are of little consequence in these results; these plots imply that if the ratio of intensities changes, interactions within the sample are taking place.

The quartz samples were too transparent to get data from the ellipsometer with. Back-surface ellipsometry was tested, though we were unable to fit models to the data. I also performed trans-

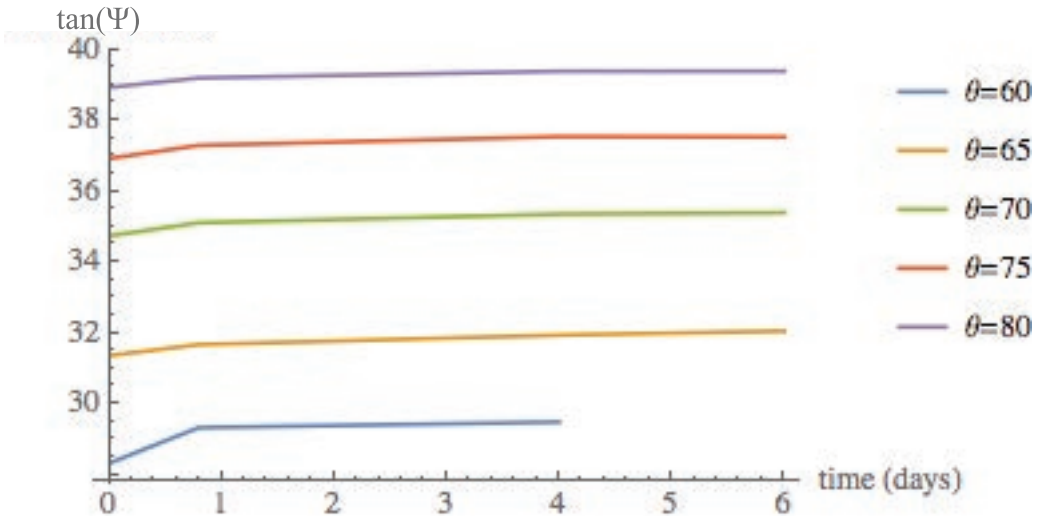


**Figure 3.1** tan(Ψ) vs. time of Sample 3 at 4.5 eV at angles $\theta = 60^o$, $65^o$, $70^o$, $75^o$, and $80^o$.

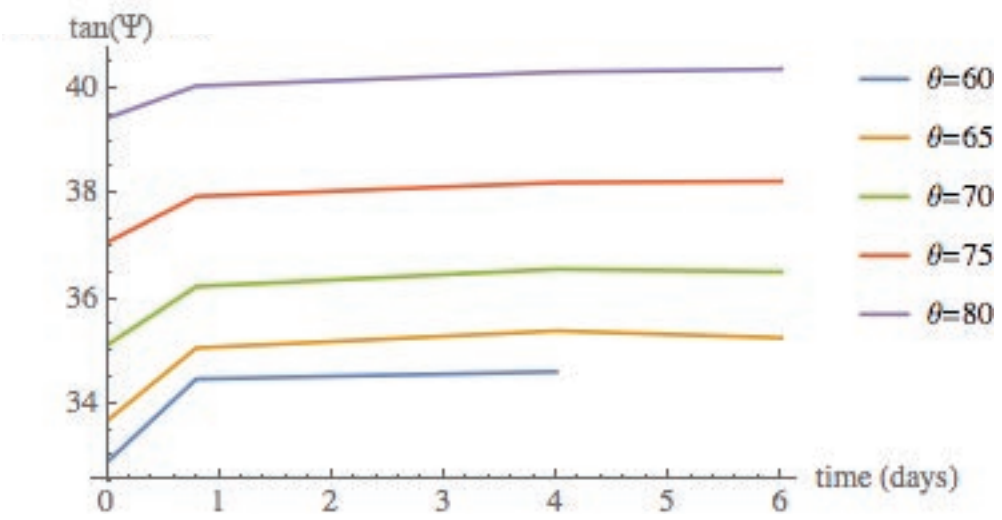


**Figure 3.2** tan(Ψ) vs. time of Sample 5 at 4.5 eV at angles $\theta = 60^o$, $65^o$, $70^o$, $75^o$, and $80^o$.

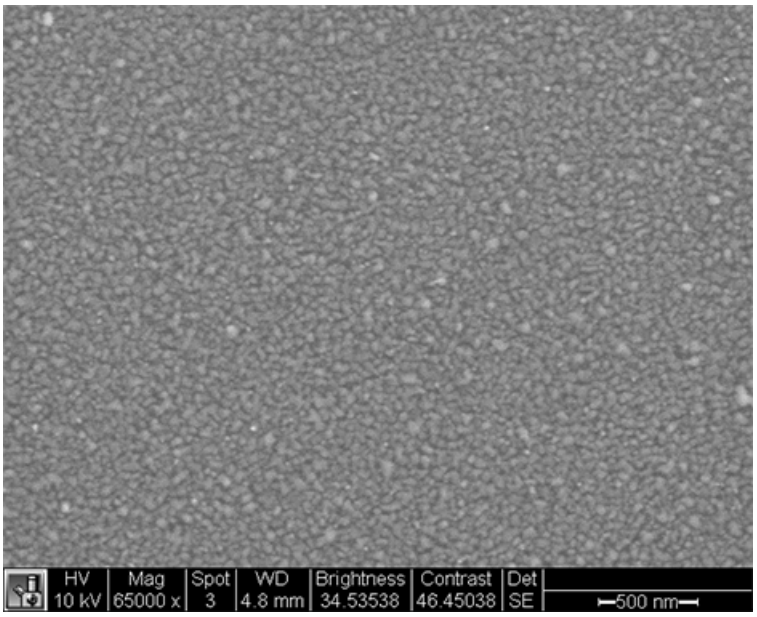


**Figure 3.3** SEM produced image of Sample 3 (Table 2.2) with beam strength 10 kV over $1.5\mu m^2$.

mission scans with the quartz samples, but the results of these are yet undeterminable.

Ellipsometry allowed me to conclude qualitatively that the samples were changing; however, it was not clear from these results how. I measured Samples 3 and 5 with SEM and EDS for more information.

Taking a closer look at Sample 3 and Sample 5, one can see the structures are relatively rough (3.3, 3.4). In the images, oddly shaped clusters of grey are spread without uniformity across the surface. These grey clusters are assumed to be Cd. Cadmium tends to clump together; one can imagine that Cd behaves similarly to Hg, which shares Group VII on the periodic table with Cd and Zn, in the way that room-temperature Hg agglomerates on a smooth surface. Although to a lesser extent, Cd also agglomerated on the surface. This poor adhesion contributed significantly to the roughness of the sample surface, ultimately leading to the inability to fit ellipsometry data to a model.

The inability to quantitatively analyze the data from the ellipsometer is not the only concern

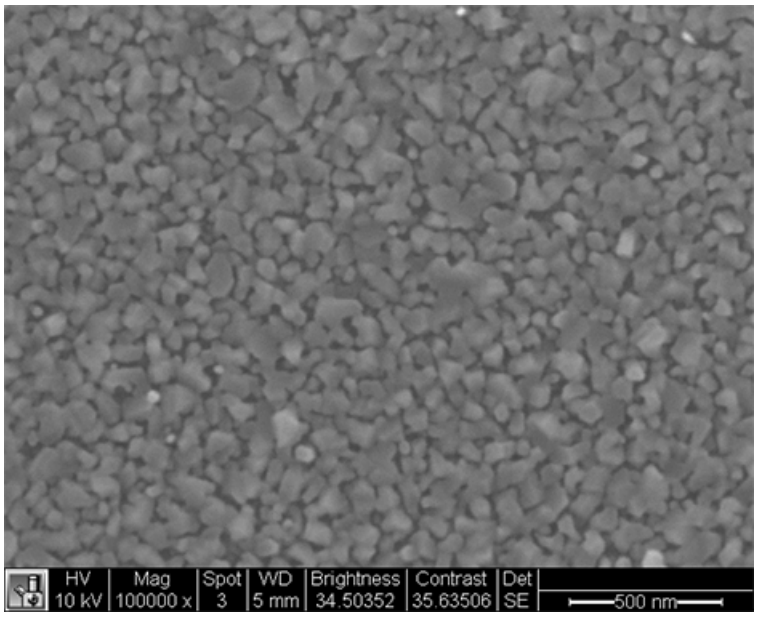


**Figure 3.4** SEM produced image of Sample 5 (Table 2.2) with beam strength 10 kV over $1.5\mu m^2$.

regarding the agglomeration of Cd. There is also cause for concern regarding Cd's capability to protect the mirrors and to be completely removed during re-evaporation. If the Cd forms clusters, as Figures 3.3 and 3.4 suggest, there are paths for O to reach the mirror. If the Cd layer is not homogenous, i.e. if some areas are thicker than others on the surface, the method of re-evaporation may prove to incompletely remove the Cd. As I will discuss in the next section, the surface inhomogeneity indeed validated this concern.

Similar structural patterns are apparent with the Zn samples. For comparison, Figure 3.5 shows the SEM image of Sample 11, which consisted of 20 nm Zn coating 10 nm Al 2.3. The image shows light grey clusters of Zn over dark grey pockets of the mirror beneath it.

Once the samples were all measured qualitatively, I needed to measure them quantitatively. Measuring sample composition with EDS yielded mixed results. The electron beam penetrated deep into the substrate, saturating the measured silicon content in the samples. EDS measures the atomic composition by percent over the target volume, providing largely unhelpful results for

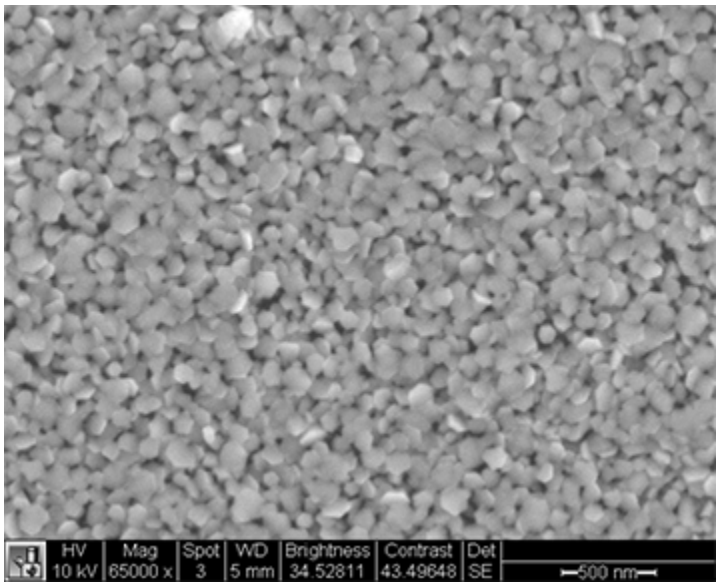


**Figure 3.5** SEM produced image of Sample 11 (Table 2.3) with beam strength 10 kV over $1.5\mu m^2$.

**Table 3.1** EDS composition results of each of the samples. The columns describe the atomic percent composition of each sample.

| Sample | 1 | 3 | 5 | 7 | 10 |
|---|---|---|---|---|---|
| Si | 35.27 | 40.08 | 39.43 | 66.79 | 31.12 |
| O | 61.58 | 0 | 0 | 30.03 | 61.18 |
| N | 0 | 57.99 | 57.11 | 0 | 0 |
| Al | 1.29 | 1.01 | 0.87 | 1.68 | 2.06 |
| Cd | 1.86 | 0.93 | 2.59 | 0 | 0 |
| Zn | 0 | 0 | 0 | 1.50 | 5.64 |

all but Sample 3 and Sample 5. These samples showed no oxygen content (3.1), suggesting that Cd may have been effective at preventing oxidation. However, the ellipsometry and SEM results suggest that some interactions occur within the samples.

Unfortunately, due to the limitations of EDS, I was unable to determine what sort of interactions were taking place. As mentioned in Chapter 2, EDS measures the percent atomic composition of the samples, not the molecular structure. In other words, it can say if there is H and O in a sample, but not if there is $H_2O$. Xray photoelectron spectroscopy (XPS) may allow for more information regarding the molecular composition of the samples; however, that is not a characterization method I was able to employ during the experiment.

The other ten of the twelve samples (all but Samples 3 and 5) were measured with EDS, but their results were accessory as they contained an interference layer of $SiO_2$. As could only be expected, EDS detected O in the samples. This is largely unhelpful, as there is no way to determine from these results whether the O is solely from the $SiO_2$ layer or if it is due as well to Al oxidation. The results for these ten samples will be set aside for further analysis (most likely XPS), but no longer discussed here.

Once the samples were characterized with ellipsometry, SEM, and EDS, pieces were broken from them and placed in the Denton for thermal re-evaporation (2.3). Of the collection of samples 'revaporated' (2.4), only Sample 5 was characterized post-REVAP.

### 3.1.2 Re-evaporation

By visual inspection, it is evident that the barrier layer of Cd in Sample 5 was unevenly removed (3.6), as suggested previously. Figure 3.6 shows Sample 5 post-REVAP. The green sections are the $SiO_2$/Si substrate, and provide a strong contrast to differentiate visually between surface composition. The grey film is the Cd barrier layer, having been removed unevenly from the Al during re-evaporation. Point A (3.7), B (3.8), and C (3.9) indicate a gradient of removal effectiveness, from most effective (Point A) to least effective (Point C).

Figures 3.7, 3.8, and 3.9 show the SEM images of Points A, B, and C from Sample 5 (3.6). At Point A, the atomic percent composition as measured by EDS indicated approximately 60%

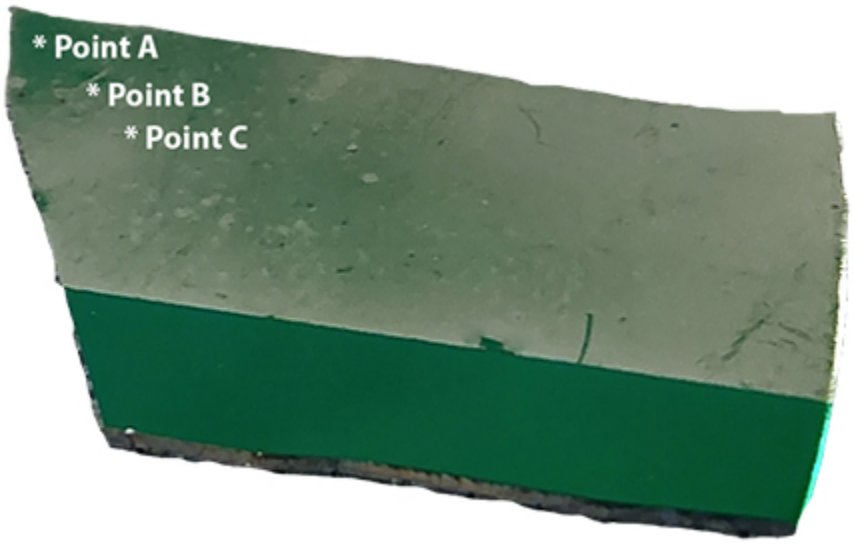


**Figure 3.6** A picture of Sample 5 after re-evaporation. Point A, B, and C indicate locations on the sample that were to be measured with EDS to determine how much Cd was removed by the re-evaporation process.

removal of Cd. Point B had approximately 36% Cd removed and Point C had approximately 28% removed. These percentages indicate that the Cd barrier layer was not evenly removed by thermal re-evaporation–at least not the way I tried to perform it.

I'll take this opportunity to segue into my last concern regarding the agglomeration of Cd: namely, where will the Cd go post-REVAP? Is it too much to assume that it will float away into the abyss, never to be seen again? Is it wise to usher a volatile, poisonous metal into space? I should say probably not. More likely, the freshly re-evaporated Cd may relocate to another component of the observatory. This could cause any number of problems that are not easily repaired in orbit.

## 3.2 Conclusions

In conclusion, the method of REVAP [4] is plausible, but requires much more experimentation before it can be used in space applications. Ellipsometry shows that interactions do occur in the

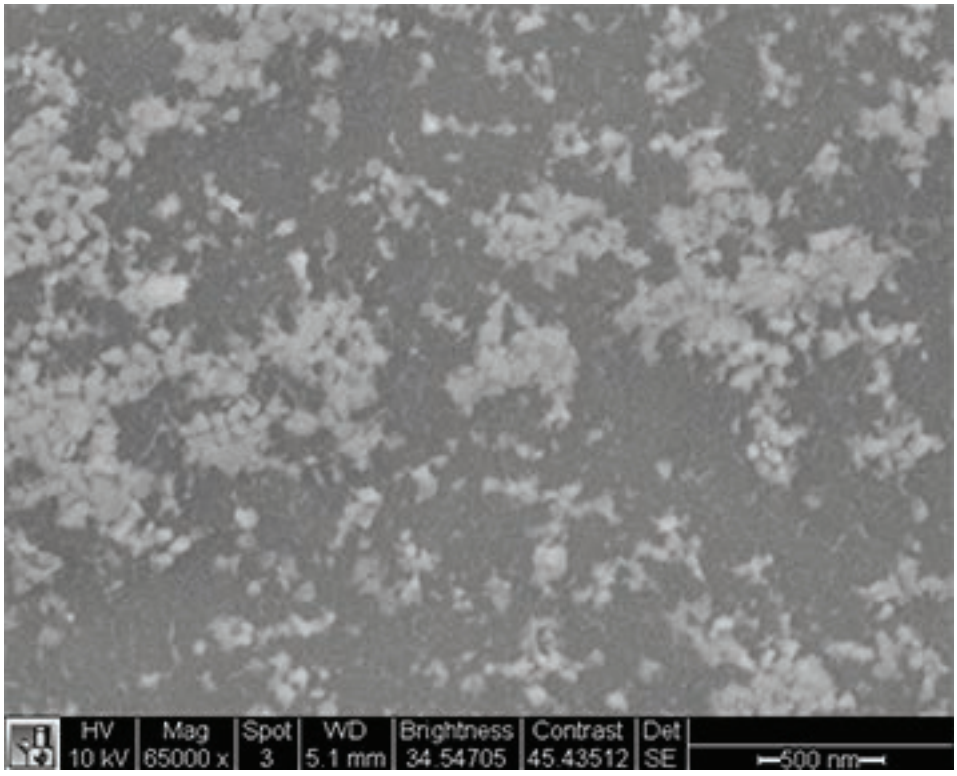


**Figure 3.7** Sample 5 post-REVAP, point C. The atomic composition of Cd removed from the sample was 60%.

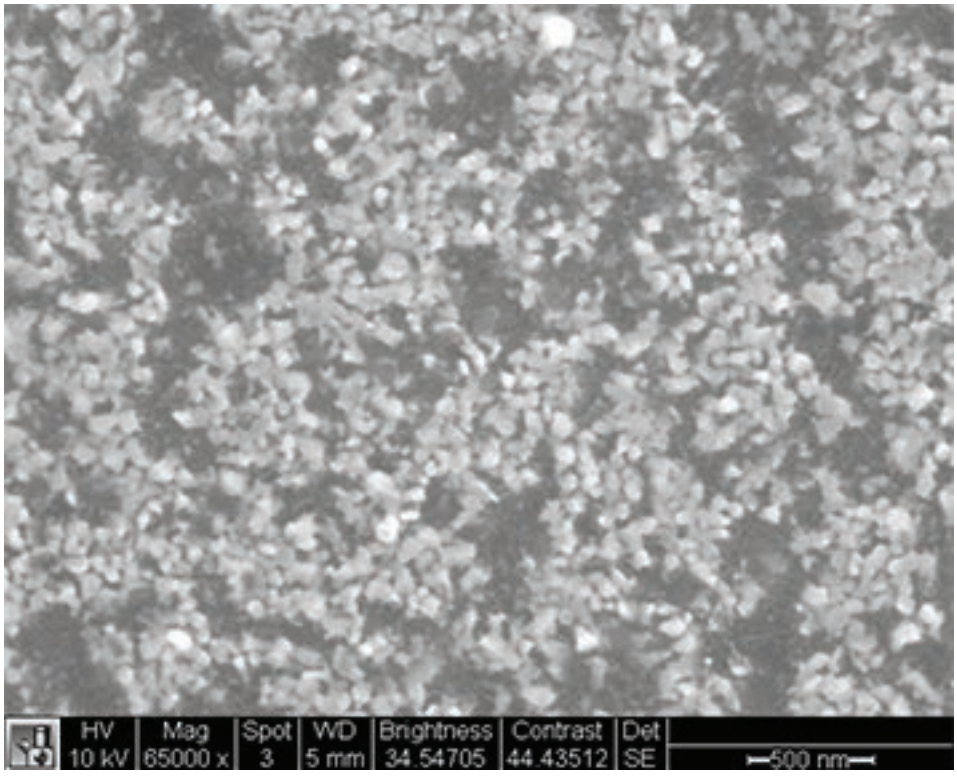


**Figure 3.8** Sample 5 post-REVAP, point B. The atomic composition of Cd removed from the sample was 36%.

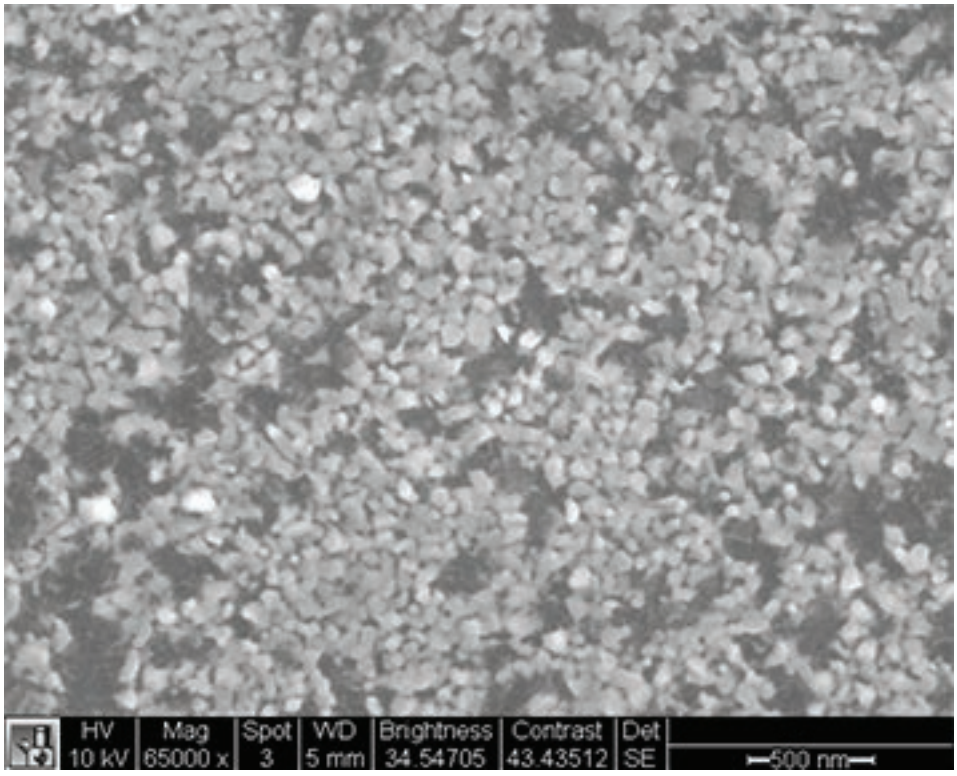


**Figure 3.9** Sample 5 post-REVAP, point C. The atomic composition of Cd removed from the sample was 28%.

protected mirrors despite the barrier layer, though it is unclear whether the interactions are due to the presence of oxygen. Images taken with SEM show rough Cd and Zn surfaces, with significant clustering of the metals. This raises the concern about opening “pathways" for O to reach the Al under the barrier layer. Composition analysis detected no O content in Sample 3 or Sample 5. In re-evaporating the samples, the method I tested proved to be inefficient and a new method ought to be considered before attempting to repeat it.

## 3.3 Further Work

My research uncovered several unexpected features of working with Al, Cd, and Zn. To proceed in this research, one should address the following issues. First, if the options for characterization do not include XPS, as mine did not, using substrates without an oxide interference layer would allow for more conclusive results with EDS. Second, the agglomerative behavior of Cd and Zn were unfavorable for this project. Oxides such as CdO and ZnO may provide better adhesion, however, EDS characterization would be compromised. CdO and ZnO have a relatively low vapor pressure compared to Al, which is a favorable feature, but they would require more care in thermal re-evaporation as they possess higher vapor pressures than pure Cd and Zn. A final suggestion for further work regards ellipsometric characterization of the samples. I used quartz samples primarily for back-surface ellipsometry, which ultimately was unsuccessful. The samples are incredibly thin (2.2, 2.3) and highly transmissive. The light did not reflect with much intensity and I was unable to fit the data to a model.

REVAP shows potential for protecting aluminized mirrors from oxidation; however, there is a need for further investigation before it can be used for space applications.

# List of Figures

# Appendix A

# Operating the Denton

The Denton allows for dual-evaporation and is well-suited to depositing metals with high vapor pressures. The main components of the Denton as identified in Figure 2.1 are (A) the stage, (B) the shutter, (C) the quartz crystal monitor, (D) the electrodes, and (E) the source.

The Denton contains two sets of electrodes, which are conducting bars of aluminum that connect with a tungsten boat, for cadmium and zinc, or coil, for aluminum. This is practical because the Al source is a thin wire that is placed in the center of the coil, while the Cd and Zn are small chunks that sit in the indention of the boat. The deposition occurs as a controlled current runs through the electrodes, generating resistance in the form of heat, and the metals are vaporized.

Everything in the chamber is coated by the evaporation, including a quartz crystal monitor. This monitor has a well-defined resonant frequency that is altered as the deposited layers add to its mass. It uses the densities of the specific evaporated materials to determine the thickness of the deposited layer. The quartz crystal monitor also controls the shutter, which blocks the stage when it is closed. Controlling the shutter allows for a predetermined nominal thickness to coat the substrate, which is positioned face-down on the stage.

Preparing the Denton for deposition required careful planning; due to their volatile nature, Cd and Zn are toxic to an evaporation deposition system. Kapton tape, a polyimide film that does not

outgas in high vacuum or leave adhesive residue upon removal, was used to protect many of the surfaces with the evaporator. Aluminum foil, a cheap and malleable material, was wrapped around the system to protect the glass bell jar.

Two vacuums reduce the pressure in the Denton. The first is a roughing pump, which brings the pressure from atmosphere to the mTorr range. A diffusion pump reduces the pressure to a workable range (in the $\mu$Torr range) and a cold trap is placed before it. It is important to note that after the depositions are completed and the diffusion pump is turned off, the roughing pump must remain running until the diffusion pump has cooled completely.

When the chamber pressure stabilizes, the deposition can begin. For the smoothest possible coating, the stage rotates the substrates above the sources. A current between $20-35\%$ of the total power runs through the electrodes, heating the Al to vaporization. Once the evaporation begins, the shutter is manually opened and the quartz crystal monitor measures the nominal thickness of the deposited Al. When the target thickness is reached, the shutter is closed and the current is shut off. The Cd and Zn are evaporated in the same way. When the deposition is complete, the chamber is vented with $N_2$ gas.

# Appendix B

# Characterization

### B.0.1 Ellipsometry

When linearly polarized light that contains both perpendicular (s-) and parallel (p-) polarization components reflects from a metal surface, it can become elliptically polarized [9]. Measuring the elliptical polarization allows for optical characterization.

Figure B.1 shows the path of linearly polarized incident light (from the left) reflecting from a surface and becoming elliptically polarized. Ellipsometry measures optical properties of a surface by sending incident light of known linear polarization to reflect from the surface of the sample,

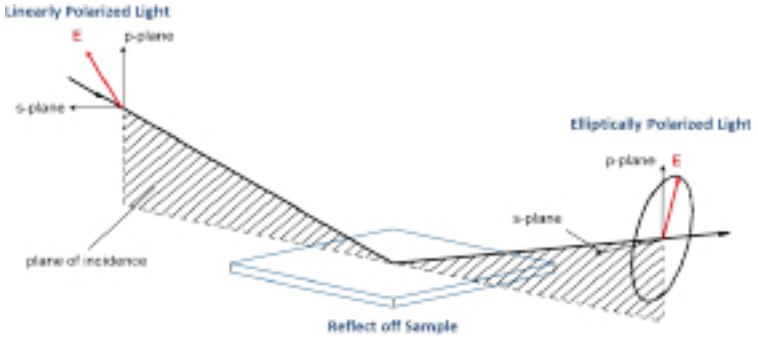


**Figure B.1** Diagram illustrating the path of the light beam of the ellipsometer. *Source: Wikipedia (Ellipsometry)*

then measures the phase shift in the reflected, elliptically polarized, light according to the Jones matrix:

$$\begin{bmatrix} \cos^2\theta & \sin\theta\cos\theta \\ \sin\theta\cos\theta & \sin^2\theta \end{bmatrix} \begin{bmatrix} -r_p & 0 \\ 0 & r_s \end{bmatrix} \begin{bmatrix} \cos\alpha \\ \sin\alpha \end{bmatrix} = \begin{bmatrix} -r_p\cos\alpha\cos^2\theta + r_s\sin\alpha\sin\theta\cos\theta \\ -r_p\cos\alpha\sin\theta\cos\theta + r_s\sin\alpha\sin^2\theta \end{bmatrix}, \tag{B.1}$$

with $\theta$ being the incident angle of the linearly polarized light, $r_p$ and $r_s$ being the Fresnel coefficients for reflection, and

$$\alpha = \frac{1}{2}\tan^{-1}\left(\frac{2AB\cos\delta}{A^2 - B^2}\right). \tag{B.2}$$

$A$ and $B$ are normalized $x$ and $y$ components of the incident electric field, $E$, defined by

$$A = \frac{|E_x|}{\sqrt{|E_x|^2 + |E_y|^2}}, \tag{B.3}$$

$$B = \frac{|E_y|}{\sqrt{|E_x|^2 + |E_y|^2}}, \tag{B.4}$$

and $\delta$ is the difference between the phase of the $E_x$ and $E_y$ components of the electric field, $\phi_y - \phi_x$. Equations B.1-B.5 are found in Peatross and Ware's *Physics of Light and Optics* [9].

I used a J. A. Woollam brand ellipsometer and the WVASE program to characterize my samples. The WVASE program measures the phase shift of the light, as described above, and the intensity of the light, which is defined as follows:

$$\tan\Psi = \sqrt{\frac{1+\xi}{1-\xi}}|\tan\alpha|, \tag{B.5}$$

with $\xi$ defined as

$$\xi = \frac{\tan^2\Psi - \tan^2\alpha}{\tan^2\Psi + \tan^2\alpha}. \tag{B.6}$$

The J.A. Woollam ellipsometer is capable of collecting data from many angles over a range of light from IR to UV ($1-7$ eV). WVASE generates a plot of energy (eV) vs. $\tan\Psi$, which can then be fit to models to identify the characteristics of the surface and layers underneath, such as the real and complex indices of refraction, layer composition, and layer thickness.

### B.0.2 Scanning Electron Microscopy

The SEM is a high-precision microscope that uses an electron beam to generate an image of a sample. At the top of the machine, a high-voltage cable causes electrons to eject from a filament. The beam is filtered through several apertures and lenses to reach the stage at the bottom. The apertures control the intensity of the light that reaches the sample and the lens control the focal length and shape of the beam. The lenses can be adjusted to correct astigmatism and refine the focus to a point on the surface. Electrons reflect from the sample at varying depths, depending on the beam strength. A beam strength of $10-15$ kV was sufficient for my samples. The reflected electrons are detected by the secondary electron detector and the backscattered electron detectors. The SEM uses reflectance angles, intensity, and other factors to project an image of a selected area of the sample. Multiple detectors are available for different purposes; a backscattered electron detector, a secondary electron detector, and an energy dispersive xray detector are three examples depicted in the schematic. The first two detectors were used to provide a picture of the surface. The third was used for EDS.

EDS provides a chemical characterization of the samples. It was performed with the SEM, but uses the energy dispersive xray detector. Xray emissions are caused when the electron beam penetrates the sample, forcing orbital transitions of bound electrons. The transitions 2p-1s (K$\alpha$), 3p-1s (K$\beta$), and 3p-2s (L$\alpha$) are the most common transitions analyzed. Each element emits photons from these orbital transitions at unique energies. For example, Cd has K$\alpha$ energy 23.106 eV, K$\beta$ energy 26.091 eV, and L$\alpha$ energy 3.133 eV [10]. Using a 10 kV electron beam, I anticipated to detect L$\alpha$ and outer-orbital transition energies (such as L$\beta$ and M$\alpha$) for Cd, but not K$\alpha$ or K$\beta$.

# Bibliography


[1] B. Sandel *et al.*, "The Extreme Ultraviolet Imager Investigation for the IMAGE Mission," Space Science Reviews **91,** 197–242 (2000).

[2] T. F. B. Sandel, "IMAGE EUV Plasmasphere Images," http://pluto.space.swri.edu/IMAGE/plasmasphere_images.html .

[3] S. Scoles, "NASA Considers Its Next Flagship Space Telescope," https://www.scientificamerican.com/article/nasa-considers-its-next-flagship-space-telescope/ (2016).

[4] W. M. Burton, "Removable volatile protective coatings for aluminised mirrors used in far-ultraviolet space astronomy," J. Phys. D: App. Phys. pp. L129–L132 (1983).

[5] L. R. C. R. P. Madden and G. Hass, "On the vacuum-ultraviolet reflectance of evaporated aluminum before and during oxidation," J. Opt. Soc. Am. pp. 620–625 (1963).

[6] M. Schmid, "Vapor Pressure Calculator," https://www.iap.tuwien.ac.at/www/surface/vapor_pressure (2013-2016).

[7] H. Thronson *et. al.*, "Path to a UV/optical/IR flagship: review of ATLAST and its predecessors," Journal of Astronomical Telescopes, Instruments, and Systems **2,** 041210 (2016).

[8] G. Hass and R. Tousey, "Reflecting Coatings for the Extreme Ultraviolet∗," J. Opt. Soc. Am. **49,** 593–602 (1959).

[9] J. Peatross and M. Ware, *Physics of Light and Optics*, 2015 ed. (available at optics.byu.edu, 2015).

[10] PANalytical, "Peak Identification Chart," (2009).

# Index